PCCP

PAPER

View Article Online
View Journal | View Issue

Cite this: *Phys. Chem. Chem. Phys.*, 2015, **17**, 21997

Unraveling the complexity of protein backbone dynamics with combined ^{13}C and ^{15}N solid-state NMR relaxation measurements†

Jonathan M. Lamley,[a] Matthew J. Lougher,[a] Hans Juergen Sass,[b] Marco Rogowski,[b] Stephan Grzesiek[b] and Józef R. Lewandowski*[a]

Typically, protein dynamics involve a complex hierarchy of motions occurring on different time scales between conformations separated by a range of different energy barriers. NMR relaxation can in principle provide a site-specific picture of both the time scales and amplitudes of these motions, but independent relaxation rates sensitive to fluctuations in different time scale ranges are required to obtain a faithful representation of the underlying dynamic complexity. This is especially pertinent for relaxation measurements in the solid state, which report on dynamics in a broader window of time scales by more than 3 orders of magnitudes compared to solution NMR relaxation. To aid in unraveling the intricacies of biomolecular dynamics we introduce ^{13}C spin–lattice relaxation in the rotating frame ($R_{1\rho}$) as a probe of backbone nanosecond-microsecond motions in proteins in the solid state. We present measurements of $^{13}C'$ $R_{1\rho}$ rates in fully protonated crystalline protein GB1 at 600 and 850 MHz ^{1}H Larmor frequencies and compare them to $^{13}C'$ R_1, ^{15}N R_1 and $R_{1\rho}$ measured under the same conditions. The addition of carbon relaxation data to the model free analysis of nitrogen relaxation data leads to greatly improved characterization of time scales of protein backbone motions, minimizing the occurrence of fitting artifacts that may be present when ^{15}N data is used alone. We also discuss how internal motions characterized by different time scales contribute to ^{15}N and ^{13}C relaxation rates in the solid state and solution state, leading to fundamental differences between them, as well as phenomena such as underestimation of picosecond-range motions in the solid state and nanosecond-range motions in solution.

Received 16th June 2015,
Accepted 17th July 2015

DOI: 10.1039/c5cp03484a

www.rsc.org/pccp

Introduction

Slow motions occurring on the nanosecond to millisecond time scale are often fundamental to protein function.[1] Solid-state NMR relaxation measurements provide an attractive method for extracting quantitative information about such motions.[2–8] Specifically, the time scales and amplitudes of ns-ms internal motions are theoretically accessible through the measurement of site-specific spin–spin (R_2) relaxation rates obtained in the solid state, which could thus provide a powerful tool to complement dynamical information available from solution studies, where the time scale of motions accessible with relaxation is limited by the correlation time of overall molecular tumbling. In practice, however, the measurement of R_2 rates in solids is difficult, as typically the measured decay rate of the transverse magnetization in a spin echo experiment ($R_2' = 1/T_2'$) is dominated by coherent contributions (*e.g.* dipolar dephasing from strongly coupled protons[9]), even in perdeuterated samples where the dense proton networks are diluted with deuterium spins.[4] In order to gain insights into dynamic transformations of biomolecules it is the incoherent R_2 (in this work referred to simply as the transverse relaxation rate) that is required, which is purely due to the stochastic modulation of local fields by molecular motion.

In solution, in the presence of chemical exchange, on-resonance $R_{1\rho}$ (spin–lattice relaxation rate in the rotating frame, $R_{1\rho} = 1/T_{1\rho}$) is a sum of pure R_2 relaxation and a scaled exchange contribution. Variation of the spin-lock field strength in $R_{1\rho}$ experiments can be used to quantify microsecond motions in solution.[10] In the solid state, it has been demonstrated for amide ^{15}N that a spin-lock field of greater strength, in combination with a magic angle spinning (MAS) frequency of more 45 kHz, may be used to decouple both the exchange contribution and any contributions from coherent processes, and hence an $R_{1\rho}$ measurement can provide a reliable estimate of incoherent R_2.[4] It is straightforward

[a] *Department of Chemistry, University of Warwick, Coventry CV4 7AL, UK. E-mail: j.r.lewandowski@warwick.ac.uk*
[b] *Biozentrum, University Basel, 4056 Basel, Switzerland*

† Electronic supplementary information (ESI) available: Additional figures and tables. Pulse sequences. Expressions for spectral densities and relaxation rates. Consideration of magic angle mis-adjustment, r.f. induced heating and polarization transfer during the $R_{1\rho}$ measurements. See DOI: 10.1039/c5cp03484a

to carry this out in a site-specific manner even in fully protonated protein samples without additional heteronuclear decoupling.[4] The $R_{1\rho}$ coherent residual is also significantly reduced in perdeuterated samples where the ^{1}H–^{1}H network is diluted.[3,11,12] Measurements of ^{15}N $R_{1\rho}$ as a function of the spin lock nutation frequency can be also used to monitor the contribution from exchange processes in solids: at spinning frequencies $\geq$60 kHz, reliable ^{15}N $R_{1\rho}$ relaxation dispersion can be obtained for nutation frequencies greater than $\sim$8 kHz in fully protonated proteins[4] and also for lower nutation frequencies in perdeuterated proteins with or without additional dilution of the exchangeable proton sites.[12,13]

Analysis of site-specific values of ^{15}N $R_{1\rho}$ measured in [U-^{13}C,^{15}N]GB1 at a single spin-lock field strength yielded order parameters and correlation times for backbone N–H vector motions, although the overall order parameters found were systematically higher than those measured using relaxation times in the solution state, if a single time scale was assumed for each amide nitrogen.[4,14] ^{15}N $R_{1\rho}$ values obtained in a similar fashion were also recently used to quantify site specific motions in Anabaena Sensory Rhodopsin.[15] Recently, a comparison of molecular dynamics (MD) simulations and ^{15}N relaxation measurements in GB1 showed that the order parameters are often dominated by slow motions and that ^{15}N R_1 (spin–lattice relaxation rates) and $R_{1\rho}$ may not be sufficient to effectively constrain the complex models required for a realistic description of protein dynamics in the solid state.[16] In general, consideration of ^{15}N relaxation alone may lead to an underestimation of the extent of backbone protein dynamics.[14] Additional relaxation parameters from ^{13}C nuclei may thus provide further valuable constraints for motional models. In particular, ^{13}C′ rates are sensitive to backbone motions with fluctuations (rotations) occurring about an axis parallel to N–H dipolar vectors, which are not detected by ^{15}N relaxation measurements. ^{13}C relaxation parameters can also provide information on side chain motions,[17] which play crucial roles in protein–protein interactions. This information should be highly complementary to ^{15}N side chain measurements that are limited to a few specific residue types such as glutamine and asparagine, which have been used to probe intermolecular interfaces in fibrils.[18]

Previously, Lewandowski *et al.* presented an approach for measuring site-specific ^{13}C spin–lattice (R_1) relaxation rates in fully protonated [U-^{13}C]-labeled proteins under $>$60 kHz spinning frequency conditions, which significantly reduce the averaging of the relaxation rates between different sites due to proton-driven spin diffusion.[19] ^{13}C′ R_1 rates measured under such conditions may be used to quantify fast and slow protein motions. However, even though the dipolar ^{13}C–^{13}C contribution to ^{13}C R_1 rates in [U-^{13}C]-labeled proteins is sensitive to slower (ns–μs) motions (as the expression for ^{13}C R_1 involves the $J(\omega_{C1} - \omega_{C2}) \approx J(0)$ spectral density[20]) other independent ^{13}C relaxation probes are desirable for achieving reliable quantitative analysis of slow dynamics.

In this manuscript we demonstrate the feasibility of measuring site-specific ^{13}C′ $R_{1\rho}$ relaxation rates as a method to probe backbone motions on ps–μs time scales in proteins in the solid state, and show how in combination with ^{13}C′ R_1 and ^{15}N R_1 and $R_{1\rho}$ measurements they may be used to quantitatively characterize those motions. The methodology presented should aid in constraining models for slow motions in proteins, and also pave the way for considering the directionality of motions.[15,21] The results that follow are organized into 5 subsections: in section (i) we investigate the validity of our method by evaluating the extent to which the coherent contributions to the measured ^{13}C $R_{1\rho}$ rates are averaged under typical experimental conditions. In section (ii), we present a comprehensive range of ^{13}C′ and ^{15}N relaxation rate measurements in crystalline [U-^{13}C,^{15}N]GB1 at 600 and 850 MHz ^{1}H Larmor frequencies. We quantify these rates in sections (iii) and (v) using models of increasing complexity. The intriguing results of the simplest model free analysis in section (iii) lead to a discussion in section (iv) on how motions with different time scales contribute to relaxation rates in the solid and solution states, highlighting fundamental differences in how dynamics influence measurements in the two phases. Our exploration provides us with hints to understanding such phenomena as the observation of very high order parameters when analyzing relaxation rates in the solid state and underestimation of nanosecond motions in solution.

Results and discussion

(i) Evaluation of coherent contributions to $R_{1\rho}$

Measured $R_{1\rho}$ relaxation rates potentially reflect not only the effect of incoherent motions, but also contributions from anisotropic NMR interactions (*e.g.* dipolar couplings) that might not be completely removed by the magic angle spinning. We first consider the magnitudes of contributions to measured $R_{1\rho}$ rates that originate from such coherent mechanisms, and the degree to which they might hamper extraction of the parameters needed for characterization of molecular motions.

Since for the ^{13}C′ nucleus the interactions contributing to the coherent residual are different from those in the previously considered case of ^{15}N,[4] it is important to assess the extent to which they are averaged under typical experimental conditions. The coherent contribution depends on the geometry of the molecular system and the extent of the MAS and radio frequency (r.f.) averaging (*e.g.* faster MAS frequencies lead to better averaging of the coherent residuals). For the same experimental set-up and similar sample geometries, the coherent contribution to ^{13}C $R_{1\rho}$ should be similar and therefore an estimate of an upper limit for this contribution under fast MAS should be obtainable from non-hydrated crystalline amino acids. Crystalline amino acid samples have similar internuclear geometries to proteins but the backbone motions and thus the relaxation rates are minimized.

To obtain such an estimate, on-resonance ^{13}C $R_{1\rho}$ rates in [U-^{13}C]glycine were measured at $\omega_r/2\pi$ = 60 kHz and $\omega_{0H}/2\pi$ = 600 MHz. Example decay curves for ^{13}C′ and ^{13}C$^{\alpha}$ (with a spin-lock pulse nutation frequency of $\omega_1/2\pi$ = 17 kHz) are shown in Fig. 1 (inset). Note that in both cases the magnetization decays very little in 0.5 s, the length of the longest employed spin-lock pulse (data points were not sampled at longer spin-lock lengths

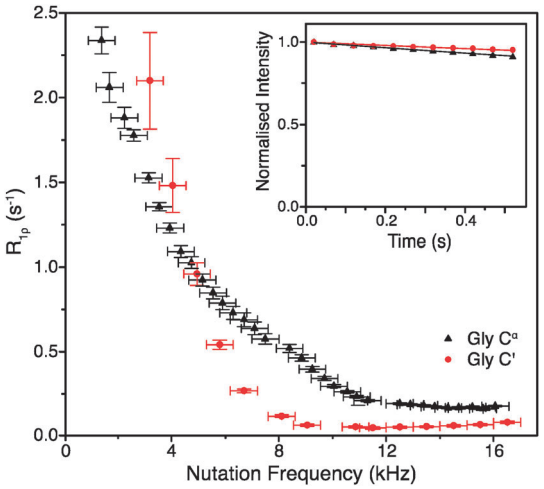

Fig. 1 $R_{1\rho}$ dispersion for $^{13}C'$ (red circle) and $^{13}C^{\alpha}$ (black triangle) in [U-^{13}C,^{15}N]glycine at $\omega_{0H}/2\pi$ = 600 MHz, $\omega_r/2\pi$ = 60 kHz, and (inset) example $R_{1\rho}$ decay curves for with $\omega_1/2\pi$ = 17 kHz.

due to hardware limitations). The main panel of Fig. 1 shows the dependence of the measured $R_{1\rho}$ rates upon the nutation frequency of the spin-lock pulse, again for both $^{13}C'$ and $^{13}C^{\alpha}$. Among the different types of carbon sites in proteins, we expect the CH_2 group to have the largest coherent contribution to ^{13}C transverse magnetization decay because of the strong proton–proton couplings present and the lack of efficient motional averaging (this is also reflected in methylene carbons being the most difficult type of carbon site geometry to decouple from protons). Even so, $R_{1\rho}$ rates for $C^{\alpha}H_2$ in glycine plateau at a value of just 0.18 ± 0.01 s^{-1} ($T_{1\rho}$ = 5.68 ± 0.32 s) for ^{13}C nutation frequencies above ~12 kHz. In the case of $^{13}C'$, where there are no directly bonded protons, the measured $R_{1\rho}$ becomes 0.06 ± 0.01 s^{-1} at nutation frequencies above ~9 kHz, corresponding to an exceptionally long $T_{1\rho}$ of 16.7 ± 2.8 s. This means that even in the "worst case" of the CH_2 group, if the decay of transverse magnetization was purely the result of coherent processes then the coherent residual for protonated ^{13}C would have an upper limit of only ~0.18 s^{-1} at 600 MHz ^{1}H Larmor frequency. Similarly, for $^{13}C'$, the residual of 0.06 s^{-1} is virtually negligible (*e.g.* <1% of the measured $^{13}C'$ average $R_{1\rho}$ in [U-^{13}C,^{15}N]GB1, see below). This suggests that much greater decay rates measured in proteins (see below) are primarily determined by contributions induced by stochastic motions. Note that the increasing $R_{1\rho}$ values for nutation frequencies <8 kHz are most likely in large part due to inadequately decoupled coherent contributions. Nevertheless, the rates at a nutation frequency of 2 kHz do not exceed 2.5 s^{-1}, which means that for cases where the exchange contributions to the rates are much larger than that value, relaxation dispersion may provide at least qualitative information about exchange processes.

Obviously, the observed $R_{1\rho}$ rates in amino acids such as glycine are not entirely due to coherent processes. In crystalline amino acids the dominant motional contribution to $^{13}C'$ relaxation originates from the rotations of CH_3 and NH_3 groups that modulate ^{1}H–$^{13}C'$ dipolar couplings.[22] As the minimal ^{1}H–$^{13}C'$ distance for both CH_3 and NH_3 groups is ~2.4 Å in glycine and alanine (and indeed the sum of all the dipolar couplings from protons <5 Å from $^{13}C'$ is almost the same), the correlation time (τ_c) of the motions should be the main differentiating factor between the relaxation behaviors of $^{13}C'$ in these amino acids.[22] The correlation time of NH_3 rotation in crystalline glycine at room temperature is shorter (~0.9 ns) than the correlation times of the rotations of both CH_3 and NH_3 groups in crystalline alanine: τ_c for CH_3 is ~1.6 ns, while for NH_3 τ_c is orders of magnitude greater.[22] The slower motions of the CH_3 and NH_3 groups in alanine are expected to cause faster $^{13}C'$ transverse relaxation than the more rapid rotation of the NH_3 group in glycine. Comparison of the $R_{1\rho}$ values measured for $^{13}C'$ in these two amino acids therefore allows further assessment of the coherent and relaxation contributions to the decay of transverse $^{13}C'$ magnetization under fast MAS conditions.

As expected from the slower correlation times for rotation of CH_3 and NH_3 groups, the measured $R_{1\rho}$'s are larger for alanine than for glycine under the same conditions, further confirming that the measured rates are almost exclusively due to relaxation induced by molecular motions. At $\omega_{0H}/2\pi$ = 600 MHz, $\omega_r/2\pi$ = 60 kHz and $\omega_1/2\pi$ = 16 kHz, the on-resonance $^{13}C'$ $R_{1\rho}$ rate for [1-^{13}C]alanine was measured at 0.83 ± 0.07 s^{-1} ($T_{1\rho}$ = 1.2 ± 0.1 s), which is 14 times larger than the value for glycine $^{13}C'$. Note that since the $R_{1\rho}$ rates observed in glycine can be quite well accounted for by the relaxation induced by the incoherent motion of NH_3 (for example, for a correlation time of 0.9 ns and an order parameter of 0.65, $^{13}C'$ and $^{13}C^{\alpha}$ $R_{1\rho}$ calculated using a simple model free approach are 0.18 and 0.06 s^{-1} respectively, *i.e.* the same as the measured rates), the coherent residuals are in reality even smaller than the values quoted above. An interesting side note is that the measured $R_{1\rho}$ of 0.18 s^{-1} for CH_2 in glycine should correspond to R_2' (minus the exchange contribution) under perfect heteronuclear decoupling conditions. Currently the smallest reported R_2' for CH_2 in glycine measured using 400 kHz SPINAL decoupling is ~4 s^{-1},[23] which is still >20 times larger than the $R_{1\rho}$ measured in this study. This result suggests that, even though it may be difficult to achieve, there is still plenty of room for improvement in heteronuclear decoupling methodology before the relaxation limit for coherence lifetimes is reached.

It should be noted that at rotary resonance and HORROR conditions ($\omega_{rf} = n\omega_r$ and $\omega_{rf} = \omega_r/2$ respectively, n = 1, 2) the coherent residual will be much larger (leading to a faster decay) due to the reintroduction of chemical shift anisotropy (CSA) and/or dipolar couplings. The experimental settings that match these conditions should either be avoided, if one is interested in the pure relaxation contribution,[11,21,24,25] or the effect should be taken directly into account.[12] As shown for the ^{15}N nucleus, larger $R_{1\rho}$ values are also observed at lower spinning frequencies due to less effective MAS averaging of the coherent residual in protonated samples (Fig. S1, ESI†).

In summary, in order to minimize the coherent contribution and obtain a reliable estimate of the incoherent R_2 for ^{13}C (including carbons with directly bonded protons) from $R_{1\rho}$ measurements in fully protonated samples, experiments should be

performed at spinning frequencies >45 kHz and employing spin-lock fields of >10 kHz with a reasonable offset from the rotary resonance and HORROR conditions. Additional experimental considerations of "mis-setting" the magic angle (small effect on the measured rate), sample heating (again moderate effect) and polarization transfer during r.f. irradiation (no significant polarization transfer due to either r.f. driven spin diffusion or isotropic mixing are observed) are addressed in the ESI† (see Fig. S2–S4).

(ii) Measurement of $^{13}C'$ and ^{15}N R_1 and $R_{1\rho}$ relaxation rates

The above discussion suggests that in hydrated proteins in the solid state, $R_{1\rho}$ rates for each individual $^{13}C'$ atom in the backbone may be measured in order to build up a dynamic picture of the molecule that should be highly complementary to that emerging from ^{15}N measurements. In this spirit, we measured site-specific $^{13}C'$ $R_{1\rho}$ for fully protonated, hydrated microcrystalline [U-^{13}C,^{15}N]GB1 at $\omega_{0H}/2\pi$ = 850 MHz and 600 MHz, with $\omega_r/2\pi$ = 60 kHz, $\omega_1/2\pi$ = 17 kHz, and a sample temperature of 27 °C. The microcrystalline protein sample was prepared as described previously.[26] In order to enhance spectral resolution the effect of one-bond C'–C^α scalar couplings was eliminated in these experiments by including an S^3E block in the pulse sequence.[27,28] The measured rates are shown in Fig. 2, along with $^{13}C'$ R_1 and amide ^{15}N R_1 and $R_{1\rho}$ measured at both fields under the same experimental conditions. All of the rates are plotted against the number of the peptide plane containing the particular ^{13}C or ^{15}N nucleus (*e.g.* peptide plane 2 refers to ^{15}N in residue 2 and $^{13}C'$ in residue 1). Rates flagged in light gray were extracted from resonances with partial overlap (see spectrum in Fig. S5 for assignments, ESI†) and thus are likely to be less accurate than those derived from fully resolved peaks. Tabulated values for the fit parameters for $^{13}C'$ and ^{15}N $R_{1\rho}$ and R_1 relaxation curves for all resonances are given in the ESI.† Table S3 (ESI†) (the average rates for 850 and 600 MHz are, respectively, $^{13}C'$ R_1 0.1 & 0.2 s^{-1}, $^{13}C'$ $R_{1\rho}$ 4.2 & 3.2 s^{-1}, ^{15}N R_1 0.05 & 0.04 s^{-1}, ^{15}N $R_{1\rho}$ 2.3 & 1.6 s^{-1}).

Upon inspection of Fig. 2 it is immediately obvious that, at both fields, the measured $^{13}C'$ $R_{1\rho}$ rates and the differences between them across different residues are one to two orders of magnitude greater than the upper limit of the coherent contribution as given by the measurement on glycine at 600 MHz (0.06 ± 0.01 s^{-1}). The rates measured in the protein are evidently almost exclusively due to relaxation induced by molecular motions. It is also clear that there is a strong correlation between rates at different fields, and generally the same features are present in both sets of data. For example, elevated rates are seen in the flexible loop and terminal regions (*e.g.* T11C′ with $R_{1\rho}$ = 14.6 ± 2.9 s^{-1} at $\omega_{0H}/2\pi$ = 850 MHz), while generally lower rates are observed in the α-helix and the central residues in β-strands with a minimum of 1.6 ± 0.4 s^{-1} for L5C′ at $\omega_{0H}/2\pi$ = 850 MHz. Our generous estimate for the upper bound of the coherent residual at $\omega_{0H}/2\pi$ = 600 MHz is in fact more than 11–14 times smaller than the mean experimental error in $^{13}C'$ $R_{1\rho}$ (0.68 s^{-1} at $\omega_{0H}/2\pi$ = 850 MHz and 0.84 s^{-1} at $\omega_{0H}/2\pi$ = 600 MHz).

While $R_{1\rho}$ and R_1 rates for both ^{15}N and ^{13}C vary significantly between residues, many features along the backbone are

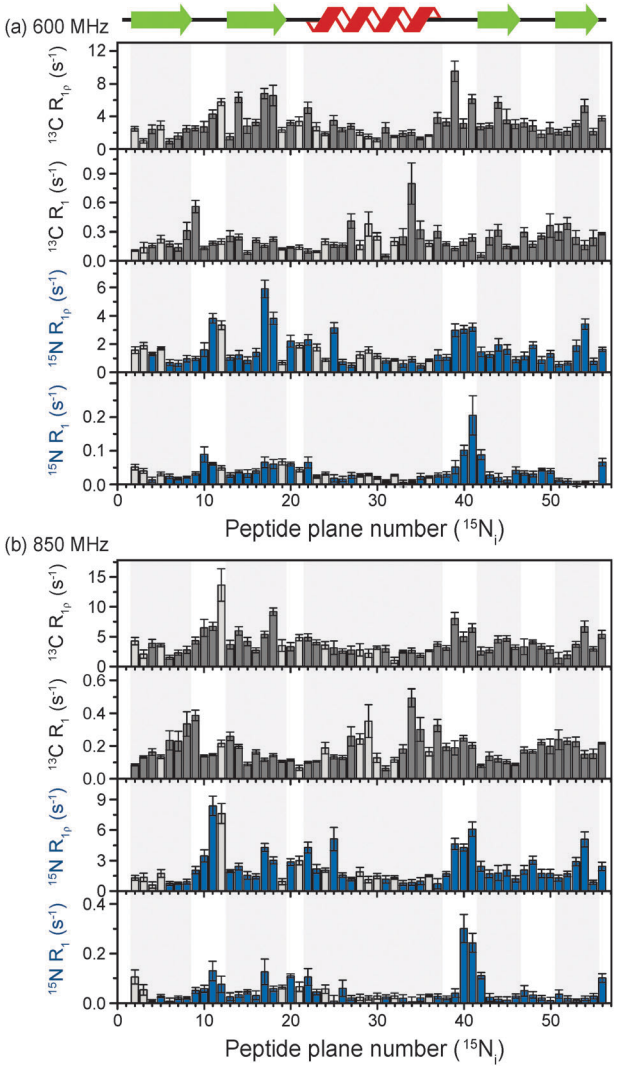

Fig. 2 $^{13}C'$ and ^{15}N R_1 and $R_{1\rho}$ relaxation rates measured on [U-^{13}C,^{15}N]GB1 as a function of peptide plane (numbering following residue number for ^{15}N). The measurements were performed at $\omega_{0H}/2\pi$ = 850 MHz and $\omega_r/2\pi$ = 60 kHz. The spin-lock nutation frequency was $\omega_1/2\pi$ = 17 kHz for both $^{13}C'$ and ^{15}N $R_{1\rho}$ measurements. Sample temperature was 27 °C for all experiments as determined by the chemical shift of water. Rates that were extracted from peaks with partial overlap are shown in light gray.

common between them (in particular for the ^{15}N and ^{13}C located in the same peptide planes, *i.e.* $^{15}N_i$ and $^{13}C_{i-1}'$, which is expected due to the rigid planar nature of the peptide bond). On the other hand, some features are apparent in the R_1 rates that are not present in the $R_{1\rho}$ rates (*e.g.* a marked increase in ^{13}C R_1 at Y33C′). This is likely due to the different dependence of these relaxation rates on the time scales of the motions causing the relaxation. Further analysis of these phenomena is carried out in the following sections *via* quantitative modeling.

(iii) Quantification of $^{13}C'$ and ^{15}N relaxation rates using the simple model free approach

To explore the influence of backbone dynamics on ^{15}N and $^{13}C'$ relaxation data in greater depth, in the following we fit our data to simple and extended model free formalism (see below).

Nuclear relaxation originates from fluctuations of local magnetic fields, caused by modulation of interactions (*e.g.* dipolar couplings or CSA) by incoherent molecular motions. Quantitative modeling of $^{13}C'$ relaxation is potentially more complex than that of ^{15}N owing to a larger number of interactions that must be included in the modeling. Whereas ^{15}N relaxation is dominated by a dipolar contribution (but with a substantial contribution from the CSA mechanism at higher fields), $^{13}C'$ relaxation, even though dominated by the CSA, may require consideration of several other contributions. For example, multiple dipolar contributions including those from C^{α}, N and nearby protons may need to be included depending on the desired precision of modeling. In particular, slow fluctuations of the dipolar C'–C^{α} vector may contribute significantly to spin–lattice relaxation, as this depends on the spectral density sampled near zero frequency which increases monotonically with the increasing correlation time of the motions. Under the conditions employed in this study the ratios between the spin-lock field strengths and frequency offsets were such that the tilt angle did not exceed 4° even at 850 MHz. The rates are therefore analyzed here as on-resonance $R_{1\rho}$ (though the effect could be easily included).

The main contributions to ^{15}N R_1 and $R_{1\rho}$ are the dipolar ^{15}N–^{1}H and ^{15}N CSA contributions:

$$R_{1,N} = R_{1,NH} + R_{1,NCSA} \quad (1)$$

$$R_{1\rho,N} = R_{1\rho,NH} + R_{1\rho,NCSA} \quad (2)$$

with

$$R_{1,NH} = \frac{1}{10}\left(\frac{\mu_0}{2\pi}\frac{\gamma_N\gamma_H}{\hbar r_{NH}^3}\right)^2 [J_0(\omega_H - \omega_N) + 3J_1(\omega_N) + 6J_2(\omega_N + \omega_H)] \quad (3)$$

$$R_{1,NCSA} = \frac{2}{15}\omega_N^2\left(\sigma_{11}^2 + \sigma_{22}^2 + \sigma_{33}^2 - \sigma_{11}\sigma_{22} - \sigma_{11}\sigma_{33} - \sigma_{22}\sigma_{33}\right) \times J_1(\omega_N) \quad (4)$$

$$R_{1\rho,NH} = \frac{1}{20}\left(\frac{\mu_0}{2\pi}\frac{\gamma_N\gamma_H}{\hbar r_{NH}^3}\right)^2 [4J_0(\omega_1) + 3J_1(\omega_N) + J_0(\omega_H - \omega_N) + 6J_1(\omega_H) + 6J_2(\omega_H + \omega_N)] \quad (5)$$

$$R_{1\rho,NCSA} = \frac{1}{45}\omega_N^2\left(\sigma_{11}^2 + \sigma_{22}^2 + \sigma_{33}^2 - \sigma_{11}\sigma_{22} - \sigma_{11}\sigma_{33} - \sigma_{22}\sigma_{33}\right) \times [4J_0(\omega_1) + 3J_1(\omega_N)] \quad (6)$$

where γ_N and γ_H are the gyromagnetic ratios of ^{15}N and ^{1}H respectively, r_{NH} is the distance between the ^{15}N and ^{1}H nuclei (here assumed to be 1.02 Å), σ are components of the ^{15}N CSA ($\sigma_{11} > \sigma_{22} > \sigma_{33}$), and J_n are the spectral densities (with rank n kept for record-keeping purposes) evaluated at the frequencies ω_X ($\omega_{H,N,C}$ are the Larmor frequencies of ^{1}H, ^{15}N and ^{13}C respectively and ω_1 is the spin-lock nutation frequency). For the modeling we use site-specific ^{15}N CSA, parameterized using ^{15}N isotropic chemical shifts (see ESI†).[29] For completeness, expressions for dipolar ^{15}N–$^{13}C'$ and ^{15}N–$^{13}C^{\alpha}$ contributions to relaxation are detailed in the ESI.†

The main contribution to $^{13}C'$ R_1 and $R_{1\rho}$ is the $^{13}C'$ CSA contribution

$$R_{1,C'\,CSA} = \frac{2}{15}\omega_C^2\left(\sigma_{11}^2 + \sigma_{22}^2 + \sigma_{33}^2 - \sigma_{11}\sigma_{22} - \sigma_{11}\sigma_{33} - \sigma_{22}\sigma_{33}\right) \times J_1(\omega_C) \quad (7)$$

and

$$R_{1\rho,C'CSA} = \frac{1}{45}\omega_C^2\left(\sigma_{11}^2 + \sigma_{22}^2 + \sigma_{33}^2 - \sigma_{11}\sigma_{22} - \sigma_{11}\sigma_{33} - \sigma_{22}\sigma_{33}\right) \times [4J_0(\omega_1) + 3J_1(\omega_C)] \quad (8)$$

where σ are orthogonal components of the $^{13}C'$ CSA ($\sigma_{11} > \sigma_{22} > \sigma_{33}$). For our modeling we used site-specific $^{13}C'$ CSA, parameterized using $^{13}C'$ isotropic chemical shifts (see ESI†).[30] Note that using other parameterizations for $^{13}C'$ and ^{15}N CSA based on solution NMR measurements on ubiquitin[31,32] generally (except for in cases where motions are characterized by low order parameters) has a very small effect on the final result in the solid state (see ESI†). In general, the results of the analysis of relaxation in the solid state are much less sensitive to the precise choice of reference dipolar couplings and CSA compared to liquid state. The expressions for more minor contributions to $^{13}C'$ relaxation, including dipolar $^{13}C'$–$^{13}C^{\alpha}$, $^{13}C'$–^{1}H, and $^{13}C'$–^{15}N contributions, are detailed in the ESI.†

A specific form of the spectral density $J(\omega)$ (*i.e.* the Fourier transform of the correlation function describing the time dependence of local magnetic field fluctuations) needs to be assumed to compute relaxation rates. In the first instance, neglecting any orientational dependence of the relaxation rates, we assume the simplest case of isotropic motion occurring on a single time scale. Accordingly, to model the relaxation rates we use the simple model free (SMF)[33,34] formalism with spectral densities expressed as

$$J(\omega) = \left(1 - S^2\right)\frac{\tau_{c,eff}}{1 + \omega^2\tau_{c,eff}^2} \quad (9)$$

where $\tau_{c,eff}$ is the effective correlation time for the motion, S^2 is an order parameter that reports on the amplitude of the motion and ω is the frequency at which the spectral density is sampled. Although this over-simplified model will not describe the motions occurring on multiple time scales, and may have shortcomings in modeling correlation functions in the solid state, which generally are non-exponential in nature,[35] it still proves to be an informative and useful approximation. In particular, in several cases considered to date, the order parameters obtained by analyzing the relaxation data either by the SMF approach (which does not take orientational dependence of relaxation rates into account) or diffusion-in-a-cone with EAS (which does take into account orientational dependence of relaxation rates) are almost the same.[24,38]

The results of the analysis of our relaxation rates using the SMF form of the spectral density, when ^{15}N and $^{13}C'$ R_1 and

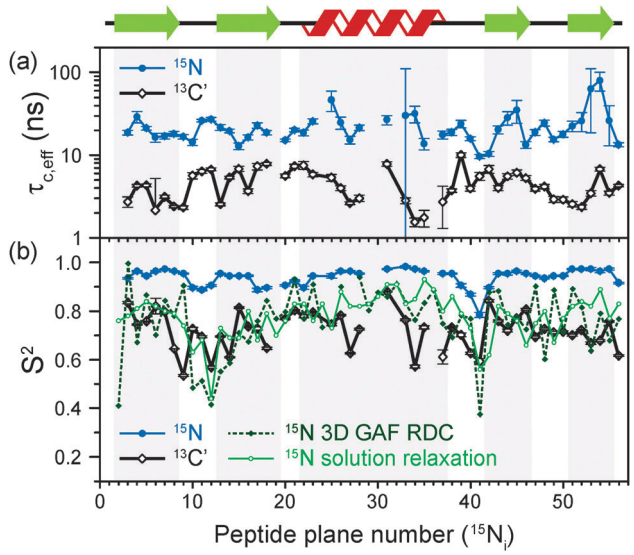

Fig. 3 Comparison of results from a simple model free (SMF) analysis of backbone motions in GB1 based on measured ^{15}N and ^{13}C′ $R_{1\rho}$ and R_1 rates (see Fig. 2): (a) correlation time ($\tau_{c,eff}$) and (b) order parameter for ^{15}N (S_{NH}^2, red circle) and ^{13}C′ ($S_{C'}^2$, black square) as a function of peptide plane number (numbering according to the residue number for ^{15}N). The short-dash blue line in (b) depicts S_{NH}^2 obtained from GB1 relaxation in solution and the green long-dash line S_{NH}^2 obtained as a result of 3D GAF analysis of RDCs in GB3.[36,37] The data for which severe peak overlap hindered accurate measurement of relaxation rates were excluded.

$R_{1\rho}$ relaxation rates are considered separately, are presented in Fig. 3. The S^2 values determined from ^{13}C′ and ^{15}N data follow similar trends but the $S_{C'}^2$ values are on average lower than S_{NH}^2 by a factor of >0.2 (Fig. 3b). The largest deviations from the overall trend are generally observed for the residues in the loops or edges of the secondary structure elements, *e.g.* peptide planes 35 to 40.

In Fig. 3b the SMF order parameters from the solid-state relaxation are also compared to the overall solution-state S_{NH}^2 derived from relaxation measurements (and thus reporting generally on <4 ns motions; light green)[36] and from residual dipolar couplings (RDC) measurements (and thus reporting on motions up to μs–ms timescale; dark green).[37] A number of studies suggest that one should expect a high level of correlation between fast picosecond-nanosecond protein motions in solution and hydrated protein crystals.[17,34,39,40] One can imagine that intermolecular interactions, *e.g.* crystal contacts, may influence slower large-scale motions to a greater extent but even though the details may vary the general motional modes are often similar.[12,41,42] Specifically for GB3, which is very similar to GB1 in terms of fold and sequence, it has been demonstrated that the pictures of dynamics in solution and hydrated crystal are very consistent over a wide range of time scales.[43] However, in a presence of more extensive specific intermolecular interactions as, *e.g.* in protein complexes, larger changes in protein dynamics may be observed; this would be true both in hydrated crystals and in solution.[13]

It is clear that the S_{NH}^2 values determined in the solid state are unusually high, if they are to be treated as the overall order parameters (*i.e.* order parameters for motions in the ps–μs range affecting the solid state relaxation rates).[4,14,16] The $S_{C'}^2$ values, however, are similar to the overall S_{NH}^2 values determined in solution except for in parts of the helix and the β_4 strand, where the $S_{C'}^2$ values are systematically lower. The effective SMF correlation times obtained from ^{13}C′ solid-state data (average $\sim$5 ns) are also systematically different from the effective correlation times obtained from ^{15}N solid-state data (average $\sim$23 ns) (see Fig. 3a).

(iv) Differences between results of SMF analyses of ^{13}C′ and ^{15}N relaxation rates

In light of the typically high level of correlation of S_{NH}^2 and $S_{C'}^2$ observed in solution NMR studies for the same peptide plane,[44] the large offset observed between such values in the solid state may appear initially perplexing. Even in the presence of anisotropic motions,[37] one would expect the order parameters and the time scales to be more similar than we observe here. As we will see in the following, the observation of the very high solid state SMF S_{NH}^2 order parameters, as well as the overall offsets between S_{NH}^2 and $S_{C'}^2$ and between the correlation times, may be understood by considering how motions occurring on different time scales contribute to the spectral densities used to calculate the relaxation rates. Such an inspection provides valuable insights into the fundamental nature of relaxation in the solid state, especially when contrasted against relaxation in the solution state.

As mentioned, the exact form of the spectral densities is model-dependent; in section (iii) we used a single time scale SMF analysis, but in general protein motions can occur on multiple time scales. Such a situation can generally be better accounted for by using an extended model free (EMF) analysis, which includes two (or more) different time scales and associated order parameters (where subscript f indicates fast and subscript s slow motion; see ESI† for further details)[34,45]

$$J(\omega) = \left(1 - S_f^2\right)\frac{\tau_f}{1+\omega^2\tau_f^2} + S_f^2\left(1 - S_s^2\right)\frac{\tau_s}{1+\omega^2\tau_s^2} \qquad (10)$$

According to a solution NMR study by Idiyatullin *et al.*, all of the residues in GB1 are characterized by both picosecond and nanosecond motions:[46] an EMF analysis yielded an average fast motion order parameter, S_f^2, of approximately 0.75, a fast motion correlation time, τ_f, on the order of tens of picoseconds, a slow motion order parameter, S_s^2, greater than 0.9 and a slow motion correlation time, τ_s, on the order of a few nanoseconds.

To assess the different contributions of these typical fast and slow motions to relaxation rates calculated by model free analyses, we simulated the spectral density terms for a fast motion (τ_f = 20 ps, S_f^2 = 0.75) and for a smaller amplitude slow motion ($10^{-11} < \tau_s < 10^{-6}$ s, S_s^2 = 0.95), using solution- and solid-state SMF formalism (see ESI,† eqn (1) and (3)). We also conducted simulations for the same motions occurring simultaneously using solution- and solid-state EMF formalism.

The results of these simulations are shown in Fig. 4, for ^{15}N in both solution and solids and for ^{13}C in solids, as a function of the correlation time of the slow motion. This figure

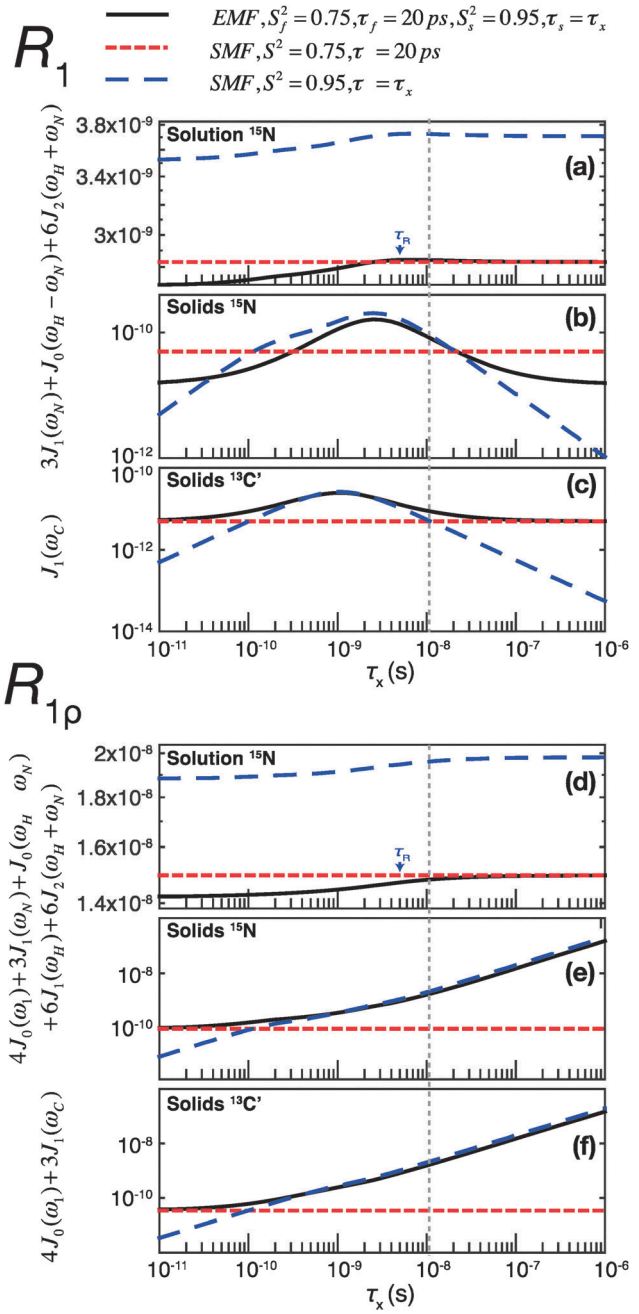

Fig. 4 Simulations of contributions of a typical fast picosecond motion and a low-amplitude slow nanosecond motion to the main contributing spectral densities to R_1 (a–c) and $R_{1\rho}$ (d–f) rates in solution and solids. (a and d) Spectral densities for ^{15}N dipolar relaxation in solution. (b and e) Spectral densities for ^{15}N dipolar relaxation in solids. (c and f) Spectral densities for ^{13}C′ CSA relaxation in solids. Red short-dashed lines represent spectral densities calculated using the SMF for a fast motion with S^2 = 0.75, τ_f = 20 ps. Blue long-dashed lines represent spectral densities calculated using the SMF for a slow motion with S_s^2 = 0.95 and τ_x as indicated on the horizontal axis. All simulations were performed with $\omega_{0H}/2\pi$ = 600 MHz. The overall rotational diffusion correlation time for the solution simulation was assumed to be 4 ns. The expressions and other parameters used for the simulations are given in the ESI.†

shows the behavior of R_1 and $R_{1\rho}$ relaxation rates calculated by an SMF treatment of pure slow motion (dashed blue line) or pure fast motion (dashed red line), as well as by an EMF treatment of both fast and slow motions simultaneously (solid black line).

Assuming the motions in GB1 occur on both ps and ns time scales,[46] the spectral densities calculated by the EMF will be more "correct", *i.e.* the calculated relaxation rates will be closer to those that would be measured experimentally given motion on those two time scales. By analyzing the same two motions separately with the SMF, we can observe how the spectral densities calculated compare to those calculated using the EMF. We can then use these observations to extrapolate to a case where the SMF is used to model a two-component motion.

Fig. 4 illustrates that the same fast and slow motions contribute differently to the spectral densities (and hence calculated relaxation rates) in the solution state and in the solid state. For EMF in the solution state, the presence of overall rotational diffusion modifies the effective correlation times for the fast and slow motions, with the result that the spectral densities (for both R_1 and $R_{1\rho}$) calculated by the EMF are similar to those calculated by the SMF including only the fast motion (see Fig. 4a and d – the black lines closely follow the dashed red lines). Conversely, in the solid state, the absence of overall tumbling means that the fast and slow motion contributions to EMF spectral densities are purely dependent on the order parameters and time scales of those motions. Compared to the solution case, this results in a greater relative contribution of slow motions to the spectral densities. For example, in the case of both ^{15}N and ^{13}C $R_{1\rho}$, the fast motion contribution to the spectral densities can be smaller than 1% of the slow motion contribution, even if S_f^2 is much lower than S_s^2. The result of this is that the $R_{1\rho}$ relaxation rates calculated by the EMF are very similar to those calculated for correlation times of >0.1 ns by the SMF using only the slow motion (see Fig. 4e and f – the black lines closely follow the dashed blue lines).

A similar situation arises for R_1 in solids: for a wide range of τ_s the contributions of the small amplitude slow motions to spectral densities are much larger than the contributions of larger amplitude fast motions. Above a certain time scale, however, the fast motion contribution begins to dominate (see Fig. 4b and c – the black line veers off toward the dashed red line above $\sim 10^{-8}$ s). Crucially, the time scale at which this occurs is shorter for ^{13}C than it is for ^{15}N. As a guide, the vertical dashed gray line indicates the slow motion time scale at which the fast motion SMF spectral densities begin to dominate over the slow motion SMF spectral densities for ^{13}C′ R_1. At this time scale (and for a range of slower time scales) the slow motion still dominates for ^{15}N. As a result, a situation can occur where the calculated ^{15}N R_1 is dominated by the slow motion component while the calculated ^{13}C′ R_1 is dominated by the fast motion component.

Consequently, in the solid state, if the SMF approach is used to analyze ^{15}N relaxation rates induced by both a fast motion and a slow motion (of *e.g.* 15 ns), the data often may be almost entirely accounted for by the slow motion only, even if the amplitude of the slow motion is small compared to that of the fast motion (an observation also made in ref. 14). In such a case, for ^{15}N a good SMF fit will be obtained with an order parameter, S_{SMF}^2, closer to the slow motion order parameter,

S_s^2, rather than the overall order parameter, $S_{overall}^2 = S_f^2 S_s^2$, and with an effective correlation time faster than the actual correlation time for the slow motion, τ_s (see also Fig. S6, ESI†). This explains why solid-state SMF analysis of ^{15}N relaxation rates in relatively rigid proteins such as GB1 and ubiquitin yields very high order parameters.[4,14] In contrast, the same nanosecond/picosecond motions would result in a much larger contribution from the fast motion for $^{13}C'$, with the determined order parameter, S_{SMF}^2, being closer to the order parameter for fast motion, S_f^2, and the effective correlation time much smaller than the correlation time for the slow motion, τ_s. This is exactly what we observe when fitting solid-state relaxation in GB1 using SMF formalism (see also Fig. S6, ESI†). Thus the offset between SMF order parameters for ^{15}N and $^{13}C'$ confirms that all residues in GB1 undergo motions on at least two distinct time scales – picosecond-range and nanosecond range or even slower.

The dominant contribution of fast picosecond motions to spectral densities in solution leads to the opposite effect to that observed in solids. Based on the analysis of synthetic data, even in the presence of small amplitude nanosecond motions, a good SMF fit can be obtained with motional parameters close to the amplitude and time scale of the fast picosecond motion (*i.e.* a single-time scale fast motion model can explain the two-time scale motion well when the slow motion has a small amplitude, because the spectral densities calculated by the EMF and SMF are similar). If the amplitude of the slow motion is much smaller than that of the fast motion then the use of EMF may not be statistically justifiable. It is likely that such a phenomenon is partially behind the fact that EMF seems to be required primarily only for modeling residues in loop regions of proteins, where the amplitudes of slow motions are sufficiently large to lead to a statistically valid improvement of an EMF fit over an SMF fit. Another consequence of this behavior is that, in solution, a large number of independent data points (*e.g.* data at several different magnetic fields) may be necessary to identify motions that are slow (but still faster than the correlation time for the overall rotational diffusion) but of relatively small amplitude. In line with these observations, recent relaxometry experiments show that nanosecond motions are likely to be significantly underestimated by the traditional EMF analysis based on solution relaxation data obtained at one or two magnetic field strengths.[47]

The above considerations of the spectral densities in the solid state have profound consequences for the interpretation of the solid-state relaxation data. Firstly, even in relatively rigid systems such as GB1, SH3 or ubiquitin, solid-state relaxation data need to be interpreted by models including multiple time scales.[2,5,48] This is also consistent with the hierarchy of protein motions established by variable temperature relaxation measurements in the solid state, where at least two motional modes with distinct activation energies were identified for backbone motions.[49] Secondly, relaxation rates alone are not sufficient to obtain a good estimate of the overall order parameter. Notably, the addition of $^{13}C'$ R_1 and $R_{1\rho}$ to the analysis of ^{15}N R_1 and $R_{1\rho}$ does not assist in obtaining a good estimate of the overall order parameter (only one parameter out of four, $^{13}C'$ R_1, is dominated by the fast motion; when weights of the data points in the fitting procedure are related to the experimental errors no special weight is given to $^{13}C'$ R_1, resulting in slow motion domination overall). Lack of sensitivity to fast motions may in fact be beneficial in certain situations, for example when modeling concerted anisotropic motions of protein fragments.[15,21] In such a case, neglecting fast picosecond motions in the fitting routine should not incur large errors for estimating the amplitudes of slow overall motions. Currently, the only way to obtain an estimate of $S_{overall}^2$ and S_f^2 is to constrain the overall amplitudes of motion by an independent measurement of dipolar couplings or CSA.[2,5,14] In the absence of an overall constraint on the order parameter, even though the relaxation rates originate from motions on multiple time scales, employing EMF is unlikely to yield realistic values for S_f^2.[14,16] A caveat of this approach is that a relatively small error in the determination of the dipolar order parameter may lead to quite a significant error in the subsequent estimate of S_f^2.[16]

(v) Extended model free analysis of peptide plane motions

The above discussion indicates that to adequately describe dynamics in crystalline GB1 using relaxation, we need to consider models involving motions occurring on at least two timescales. In case of crystalline SH3, Zinkevich *et al.* argued that often three time scales are required.[48] In another study,[13] we found that only a handful of residues exhibit microsecond-scale motions based ^{15}N $R_{1\rho}$ relaxation dispersion (clear dispersion is observed for residues 17, 19, 20, 44, 46, 49–53; note that the microsecond motions for these residues are likely too slow to effectively influence the measured dipolar order parameter), suggesting that for the majority of residues the dynamics can be well-described by motions in the ps-ns range. Note that data informing on millisecond-scale motions are currently not available. For motions in this range of time scales, measurements of dipolar couplings may be used to constrain the overall amplitude of motions (in general, dipolar couplings are averaged by motions faster than their inverse) and the expressions for $R_{1\rho}$ presented above can be used without including the influence of spinning frequency,[24] which should generally be included if the motions in the μs–ms regime are present (see ESI†).

First, to establish our baseline, we performed a fit using only ^{15}N R_1 and $R_{1\rho}$ data measured at 600 MHz and 850 MHz magnetic fields, with dipolar NH order parameters[16,29] used to constrain the overall amplitude of motions. This scheme represents roughly the current state of the art in the literature.[2,5,14,48,50] To model ^{15}N relaxation we have included dipolar contributions from the directly bonded proton, C^α and C', site-specific ^{15}N CSA (see ESI†), and dipolar contributions from other protons implemented as an additional effective NH coupling.[51] The results of the fits are presented in Fig. 5 (black diamonds and lines). The emerging picture of the dynamics in crystalline GB1 is consistent with similar analyses on other model crystalline systems such as SH3 and ubiquitin: all residues seem to be characterized by larger amplitude picosecond motions and smaller amplitude (order parameters close to 1) slow motions with a correlation time in the ns–μs range. Only a few of residues in

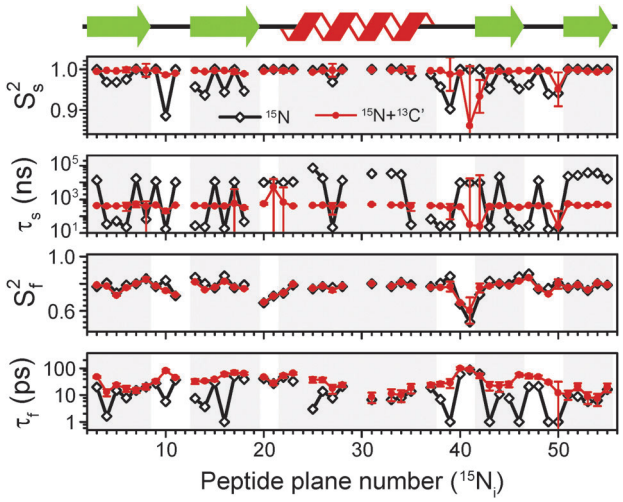

Fig. 5 Comparison of an extended model free (EMF) analysis of backbone dynamics based on ^{15}N R_1 and $R_{1\rho}$ relaxation (black line) and combined ^{15}N R_1 and $R_{1\rho}$ and ^{13}C′ R_1 and $R_{1\rho}$ relaxation for the sites in the same peptide planes (red line). S_s^2, τ_s, S_f^2, τ_f are, respectively: order parameter for the slow motion (reflecting amplitude of motion), correlation time for the slow motion, order parameter for the fast motion and correlation time for the fast motion. Measurements performed both at 600 and 850 MHz spectrometers were used in both cases. The overall amplitude of motion was constrained by measurements of NH dipolar couplings, which are averaged by motions faster than the inverse of its rigid limit value. The data for which NH dipolar couplings were not available or for which severe peak overlap hindered accurate measurement of relaxation rates were excluded.

loops exhibit larger than average slow motions. Notably, the order parameters for the fast picosecond motions are on average similar to the overall order parameters for GB1/GB3 in solution,[36,46,52] providing yet another example that indicates the overall high level of similarity of fast picosecond dynamics for globular proteins in solution and in hydrated crystals.[34]

In spite of this reassuringly familiar view of GB1 dynamics, there are a few points of concern: for a number of residues the fast correlation times are in the low-picosecond regime (or at the 1 ps bound imposed in the fitting procedure; several such points were also found in a recent EMF analysis of ^{15}N relaxation in ubiquitin[14]) and for the majority of the residues slow correlation times are in the microsecond regime. Both of these features are likely to be fitting artifacts, with the data not providing sufficient basis for an accurate description of the dynamics. Motions with correlation times of a few picoseconds have a negligible effect on the measured relaxation rates and as such these kinds of motions are unlikely to be accurately determined from relaxation measurements. On the other hand, the omnipresence of microsecond motions is inconsistent with the lack of microsecond exchange as demonstrated by ^{15}N $R_{1\rho}$ relaxation dispersion in crystalline GB1[13] (similarly, in ubiquitin a few residues, *e.g.* 10, 44, 63, were found where microsecond motions were detected through an EMF analysis of ^{15}N relaxation rates but not confirmed in ^{15}N relaxation dispersion[12,14]). An examination of the determined parameters reveals that for many residues, the parameters for the fast motion are such that they have negligible contributions to $R_{1\rho}$ and the parameters for the slow motions have negligible contributions to R_1. These results suggest that even though the considered data set is sufficient to obtain fairly reasonable estimates of the amplitudes of motion, it is not sufficient to provide accurate determination of time scales of motions.

This situation may improve as data measured at a larger number of magnetic fields, or at least much more different magnetic fields, is available to provide better sampling of the spectral density at different frequencies. Indeed, if we include ^{15}N R_1 and $R_{1\rho}$ previously measured at a magnetic field of 1000 MHz,[4] the "artifactual" microsecond slow motions and 1 ps fast motions are eliminated for several residues (see ESI†). For many others, however, microsecond motions are still detected, in direct disagreement with the relaxation dispersion data. The situation is not greatly improved by using the expressions for $R_{1\rho}$ that explicitly include spinning frequency effects (see ESI†).[24]

A potential solution to this problem could be to supplement the data with measurements that allow, at the same magnetic fields, to sample spectral densities at very different frequencies, for example ^{13}C′ data. Typically, in solution, order parameters for ^{15}N and ^{13}C′ in the same peptide planes are highly correlated, with only a slight offset between them.[44] This is expected because due to the planarity of the peptide bond ^{15}N and ^{13}C′ are likely to undergo similar motions. Even though such motions are expected to be anisotropic in nature,[37,44] to the first approximation data can be treated reasonably well by assuming isotropic fluctuations of the peptide planes.[44]

Following the assumption of isotropic peptide plane motions we refitted the data, adding ^{13}C′ R_1 and $R_{1\rho}$ data at 600 MHz and 850 MHz magnetic fields to the EMF analysis. To model ^{13}C′ relaxation we included site-specific ^{13}C′ CSA, dipolar contributions from the couplings to C^α, N and H^N, and dipolar contributions from other protons implemented as an additional effective ^{13}C′–^{1}H coupling[51] (see ESI†). The results of the combined ^{13}C′ and ^{15}N fits (red circles and lines) are depicted in Fig. 5, where they are overlaid with the results of analysis based on ^{15}N data only. For most residues, the changes in order parameters upon inclusion of ^{13}C′ relaxation rates in the analysis are relatively small. However, there is a pronounced effect on the determined time scales. In particular, the slow correlation times are less than 1 μs for most residues (average ~500 ns), in line with the results of ^{15}N relaxation dispersion. The overall fairly consistent time scale for slow motions in the secondary structure elements (very different time scales only appear in the loops) may be suggestive of an overall small amplitude motion.[21] A few resonances for which clear relaxation dispersion is observable may require a model that includes motions occurring on three time scales but it is not entirely obvious how one could constrain their amplitude. In addition, the artifactual low picosecond motions are removed and the overall trend of time scales along the protein backbone varies more "smoothly" from residue to residue. Interestingly, the determined fast correlation times become overall similar to the fast correlation times determined in GB1 under similar conditions in solution, which, together with similar S_f^2 (ref. 36) (see ESI†), again further highlighting the similarity of fast dynamics in solution and hydrated crystals.

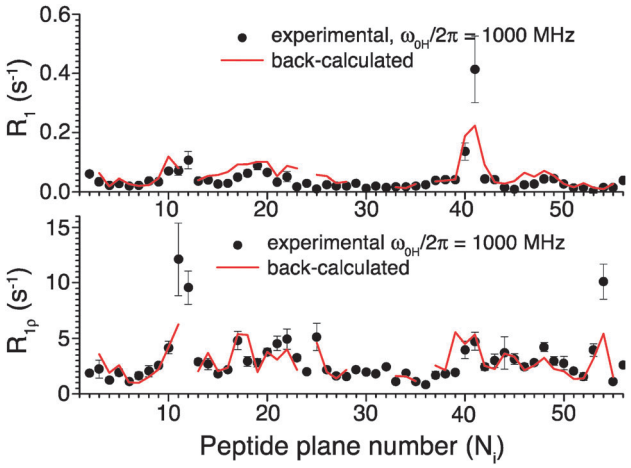

Fig. 6 Comparison of ^{15}N R_1 and $R_{1\rho}$ relaxation rates measured in crystalline GB1 at 1 GHz ^{1}H Larmor frequency (black points)[4] and those back-calculated from an EMF analysis based on ^{15}N and ^{13}C′ relaxation rates measured at 600 and 850 MHz ^{1}H Larmor frequencies in Fig. 5 (red line).

To further validate the obtained picture of GB1 dynamics, we back-calculated ^{15}N R_1 and $R_{1\rho}$ rates for 1000 MHz ^{1}H Larmor frequency based on the EMF analysis of 600 and 850 MHz data and compared them in Fig. 6 to previously-measured experimental values.[4] In spite of the fact that the measurements at 1000 MHz were not conducted at the exact same temperature as those at 600/850 MHz, the back-calculated values agree reasonably well with the experimental values (see ESI†).

It might be useful to highlight that the results of the performed analyses are not greatly affected by the precise choice of bond length and CSA magnitude. In the solid state, relatively large changes in bond lengths of CSA have minimal effects on the results of model free analysis of relaxation rates. For example, regardless of whether r_{NH} = 1.02 Å or r_{NH} = 1.04 Å is used to model the ^{15}N relaxation, the obtained order parameters and correlation times are virtually the same except for cases of large amplitude motions (see ESI†). This observation relates to the fact that in the solid state in a presence of slow motions small changes in order parameters lead to large changes in $R_{1\rho}$, in fact, the dependence of rate on order parameter is much steeper than the dependence on bond length or CSA magnitude. In contrast, in solution the effect of such slow motions is effectively "truncated" by the overall rotational diffusion leading to a reverse situation where the dependence of the rates on bond length or CSA magnitude is steeper than the dependence on order parameter. As a result, even though the amplitudes of motions determined from the analysis of relaxation rates in solution may vary significantly depending on the precise choice of magnitude for modulated interactions, the amplitudes of motions determined from the analysis of relaxation rates in solid state will be affected to a lesser degree by similar variations. To model ^{15}N and ^{13}C′ CSA relaxation we used here site-specific values obtained from a model where the CSA tensor was parameterized using isotropic chemical shift and based on measurements performed on crystalline GB1. However, in the performed model free analysis the use of other models of CSA (*e.g.* similar parameterizations obtained from measurements on ubiquitin in solution, or generic average CSA) has only a small effect on the obtained results (again except when large amplitude motions are concerned). Such a difference in behavior between solution and solid-state relaxation analysis traces back, again, to the forms of spectral densities and the absence of the dominant term from overall rotational diffusion in the solid state.

Experimental

NMR experiments were conducted on a Bruker Avance III spectrometer operating at 20.0 T ($\omega_{0H}/2\pi$ = 850 MHz) and a Bruker Avance II+ spectrometer operating at 14.1 T ($\omega_{0H}/2\pi$ = 600 MHz), using a Bruker 1.3 mm triple-resonance probe at each field. Unless otherwise stated, experiments were performed at 60 kHz MAS frequency, at a sample temperature of 27.0 ± 0.5 °C as measured by the ^{1}H chemical shift of water with respect to DSS.[53] The pulse sequence used to collect ^{13}C′ $R_{1\rho}$ rates (Fig. S10a, ESI†) was based on a standard NCO double-CP (DCP[54]) sequence followed by a spin-lock pulse on the carbon channel whose length was incremented across each series of experiments. An S^{3}E block[27] was added to enhance resolution in the direct dimension by removing the effect of one-bond C′–C$^\alpha$ scalar couplings. A similar sequence (but with the spin-lock pulse instead on the ^{15}N channel, before the indirect acquisition (t_1) period) was used to measure site-specific backbone amide ^{15}N $R_{1\rho}$ rates (see Fig. S10, ESI†). For all ^{13}C′ and ^{15}N $R_{1\rho}$ experiments (unless otherwise stated), the spin-lock nutation frequency was set to 17 kHz, calibrated using nutation spectra. Nutation spectra also allowed us to determine the average r.f. inhomogeneity, which was on the order of 15%.

^{13}C and ^{15}N R_1 rates were measured using sequences based on a standard NCO, but with a delay period (directly before t_1 acquisition for ^{15}N R_1, directly after ^{15}N–^{13}C CP for ^{13}C′ R_1) that was incremented between experiments. π/2 pulses were applied either side of this delay (100 kHz on ^{13}C for ^{13}C′ R_1, 83.3 kHz on ^{15}N for ^{15}N R_1). All sequences are given in Fig. S10 (ESI†). The Bruker pulse sequences are available from the authors' website.

All sequences were initialized with a 100 kHz π/2 ^{1}H pulse, followed by adiabatic double quantum cross-polarization[55] from ^{1}H to ^{15}N (1.5 ms, $\omega_{1H}/2\pi \approx$ 50 kHz, $\omega_{1N}/2\pi$ = 10 kHz). After t_1 evolution, magnetization was transferred to ^{13}C by a second adiabatic CP (9 ms, $\omega_{1N}/2\pi \approx$ 50 kHz, $\omega_{1C}/2\pi$ = 10 kHz). During t_1 ($t_{1,max}$ = 10 ms) and t_2 (40 ms at 850 MHz, 25 ms at 600 MHz) acquisition, slpTPPM decoupling[19] was applied at a field strength of ~15 kHz.

Spectra were processed with TopSpin 2.1, and the relaxation series were subsequently analysed using CcpNmr Analysis 2.2.2. Final relaxation curve fitting was completed in Matlab. Data were fitted to $I_0 \exp(-Rt)$, with I_0 and R being the fit parameters.

Fitting of the relaxation data to SMF and EMF was performed in Matlab. All the expressions for the rates, spectral densities as well as magnitudes of interactions are detailed in the ESI.† The minimization was performed using code based on the fminsearch function with several random starting points

to ensure a global minimum was found. The best-fit amplitude and time scale parameters for all the models were determined by minimizing the χ^2 target function:

$$\chi^2 = \sum_i \frac{\left(X_{i,\mathrm{calc}} - X_{i,\mathrm{exp}}\right)^2}{{\sigma_{i,\mathrm{exp}}}^2} \quad (11)$$

where X_i are relaxation rates and dipolar coupling measurements, σ_i appropriate experimental errors. The rigid limit NH distance was assumed to be 1.02 Å. Errors for the EMF amplitudes and time scales were estimated using Monte Carlo error analysis using 1000 iterations. Briefly, relaxation rates were back-calculated from the best fit parameters, random noise within the bounds of experimental error was added to the rates and the resulting rates fitted to the model. This procedure was repeated 1000 times and the error set at a two times the standard deviation of the results from all the runs.

Conclusions

In summary, we have introduced ^{13}C $R_{1\rho}$ measurements as a robust quantitative probe of slow protein motions in the solid state that is highly complementary to ^{15}N relaxation measurements. We showed that solid-state $R_{1\rho}$ rates are exceedingly sensitive to even very small-amplitude slow conformational changes. A comparison of simple model free analyses of ^{15}N and ^{13}C′ R_1 and $R_{1\rho}$ data illustrated that relaxation in GB1 in solid state is in general induced by motions occurring on multiple time scales, but usually dominated by the slower nanosecond-range motions. Analyzing the differences between solution- and solid-state spectral densities, we could explain why very high order parameters are obtained from simple model free analyses of ^{15}N relaxation in the solid state, and why nanosecond motions are likely to be underestimated in a standard relaxation analysis of solution NMR relaxation data. We also showed that by combining ^{15}N and ^{13}C′ relaxation data it is possible to obtain a more physically meaningful dynamical description of proteins that is highly complementary to the picture provided by other techniques. Finally, combining ^{15}N and ^{13}C′ measurements in such a manner paves the way to considering anisotropic peptide plane motions, which will be considered in a future manuscript.

Acknowledgements

We thank Dr Dinu Iuga for the assistance with acquiring data at the UK 850 MHz Solid-state NMR Facility. We thank Prof. Steven Brown for providing the crystalline amino acid samples. JML and MJL acknowledge support of the EPSRC. JRL acknowledges support of Research Development Fund from University of Warwick, EPSRC grant EP/L025906/1 and BBSRC grant BB/L022761/1. The UK 850 MHz Solid-state NMR Facility used in this research was funded by EPSRC and BBSRC, as well as the University of Warwick, including part funding through Birmingham Science City Advanced Materials Projects 1 and 2 supported by Advantage West Midlands (AWM) and the European Regional Development Fund (ERDF). SG acknowledges funding by the Swiss National Science Foundation grant 310030_149927. Raw NMR data and Matlab scripts used for the analysis can be obtained from the authors upon request.

Notes and references

1 K. Henzler-Wildman and D. Kern, *Nature*, 2007, **450**, 964–972.
2 V. Chevelkov, U. Fink and B. Reif, *J. Biomol. NMR*, 2009, **45**, 197–206.
3 A. Krushelnitsky, T. Zinkevich, D. Reichert, V. Chevelkov and B. Reif, *J. Am. Chem. Soc.*, 2010, **132**, 11850–11853.
4 J. R. Lewandowski, H. J. Sass, S. Grzesiek, M. Blackledge and L. Emsley, *J. Am. Chem. Soc.*, 2011, **133**, 16762–16765.
5 P. Schanda, B. H. Meier and M. Ernst, *J. Am. Chem. Soc.*, 2010, **132**, 15957–15967.
6 M. Tollinger, A. C. Sivertsen, B. H. Meier, M. Ernst and P. Schanda, *J. Am. Chem. Soc.*, 2012, **134**, 14800–14807.
7 J. J. Helmus, K. Surewicz, W. K. Surewicz and C. P. Jaroniec, *J. Am. Chem. Soc.*, 2010, **132**, 2393–2403.
8 J. Yang, M. L. Tasayco and T. Polenova, *J. Am. Chem. Soc.*, 2009, **131**, 13690–13702.
9 K. Schmidt-Rohr and H. W. Spiess, *Multidimensional solid-state NMR and polymers*, Academic Press, London, 1994.
10 A. Mittermaier and L. E. Kay, *Science*, 2006, **312**, 224–228.
11 C. M. Quinn and A. E. McDermott, *J. Magn. Reson.*, 2012, **222**, 1–7.
12 P. Ma, J. D. Haller, J. Zajakala, P. Macek, A. C. Sivertsen, D. Willbold, J. Boisbouvier and P. Schanda, *Angew. Chem., Int. Ed. Engl.*, 2014, **53**, 4312–4317.
13 J. M. Lamley, C. Oster and J. R. Lewandowski, unpublished.
14 J. D. Haller and P. Schanda, *J. Biomol. NMR*, 2013, **57**, 263–280.
15 D. B. Good, S. Wang, M. E. Ward, J. Struppe, L. S. Brown, J. R. Lewandowski and V. Ladizhansky, *J. Am. Chem. Soc.*, 2014, **136**, 2833–2842.
16 L. Mollica, M. Baias, J. R. Lewandowski, B. J. Wylie, L. J. Sperling, C. M. Rienstra, L. Emsley and M. Blackledge, *J. Phys. Chem. Lett.*, 2012, **3**, 3657–3662.
17 V. Agarwal, Y. Xue, B. Reif and N. R. Skrynnikov, *J. Am. Chem. Soc.*, 2008, **130**, 16611–16621.
18 J. R. Lewandowski, P. C. A. van der Wel, M. Rigney, N. Grigorieff and R. G. Griffin, *J. Am. Chem. Soc.*, 2011, **133**, 14686–14698.
19 J. R. Lewandowski, J. Sein, H. J. Sass, S. Grzesiek, M. Blackledge and L. Emsley, *J. Am. Chem. Soc.*, 2010, **132**, 8252–8254.
20 T. Yamazaki, R. Muhandiram and L. E. Kay, *J. Am. Chem. Soc.*, 1994, **116**, 8266–8278.
21 J. R. Lewandowski, J. Sein, M. Blackledge and L. Emsley, *J. Am. Chem. Soc.*, 2010, **132**, 1246–1248.
22 A. Naito, S. Ganapathy, K. Akasaka and C. A. Mcdowell, *J. Magn. Reson.*, 1983, **54**, 226–235.
23 S. K. Vasa, H. Janssen, E. R. H. Van Eck and A. P. M. Kentgens, *Phys. Chem. Chem. Phys.*, 2011, **13**, 104–106.
24 R. Kurbanov, T. Zinkevich and A. Krushelnitsky, *J. Chem. Phys.*, 2011, **135**, 184104.

25 C. M. Quinn and A. E. McDermott, *J. Biomol. NMR*, 2009, **45**, 5–8.
26 W. T. Franks, D. H. Zhou, B. J. Wylie, B. G. Money, D. T. Graesser, H. L. Frericks, G. Sahota and C. M. Rienstra, *J. Am. Chem. Soc.*, 2005, **127**, 12291–12305.
27 S. Laage, A. Lesage, L. Emsley, I. Bertini, I. C. Felli, R. Pierattelli and G. Pintacuda, *J. Am. Chem. Soc.*, 2009, **131**, 10816–10817.
28 I. Bertini, L. Emsley, I. C. Felli, S. Laage, A. Lesage, J. R. Lewandowski, A. Marchetti, R. Pierattelli and G. Pintacuda, *Chem. Sci.*, 2011, **2**, 345–348.
29 B. J. Wylie, L. J. Sperling, A. J. Nieuwkoop, W. T. Franks, E. Oldfield and C. M. Rienstra, *Proc. Natl. Acad. Sci. U. S. A.*, 2011, **108**, 16974–16979.
30 B. J. Wylie, L. J. Sperling, H. L. Frericks, G. J. Shah, W. T. Franks and C. M. Rienstra, *J. Am. Chem. Soc.*, 2007, **129**, 5318–5319.
31 K. Loth, P. Pelupessy and G. Bodenhausen, *J. Am. Chem. Soc.*, 2005, **127**, 6062–6068.
32 P. R. L. Markwick and M. Sattler, *J. Am. Chem. Soc.*, 2004, **126**, 11424–11425.
33 G. Lipari and A. Szabo, *J. Am. Chem. Soc.*, 1982, **104**, 4546–4559.
34 V. Chevelkov, A. V. Zhuravleva, Y. Xue, B. Reif and N. R. Skrynnikov, *J. Am. Chem. Soc.*, 2007, **129**, 12594–12595.
35 D. A. Torchia and A. Szabo, *J. Magn. Reson.*, 1982, **49**, 107–121.
36 J. J. Barchi, B. Grasberger, A. M. Gronenborn and G. M. Clore, *Protein Sci.*, 1994, **3**, 15–21.
37 G. Bouvignies, P. Bernado, S. Meier, K. Cho, S. Grzesiek, R. Bruschweiler and M. Blackledge, *Proc. Natl. Acad. Sci. U. S. A.*, 2005, **102**, 13885–13890.
38 M. J. Knight, A. J. Pell, I. Bertini, I. C. Felli, L. Gonnelli, R. Pierattelli, T. Herrmann, L. Emsley and G. Pintacuda, *Proc. Natl. Acad. Sci. U. S. A.*, 2012, **109**, 11095–11100.
39 H. B. Cole and D. A. Torchia, *Chem. Phys.*, 1991, **158**, 271–281.
40 A. Tamura, M. Matsushita, A. Naito, S. Kojima, K. I. Miura and K. Akasaka, *Protein Sci.*, 1996, **5**, 127–139.
41 G. L. Olsen, M. F. Bardaro, D. C. Echodu, G. P. Drobny and G. Varani, *J. Biomol. NMR*, 2009, **45**, 133–142.
42 J. C. Williams and A. E. McDermott, *Biochemistry*, 1995, **34**, 8309–8319.
43 G. M. Clore and C. D. Schwieters, *J. Mol. Biol.*, 2006, **355**, 879–886.
44 S. L. Chang and N. Tjandra, *J. Magn. Reson.*, 2005, **174**, 43–53.
45 G. M. Clore, A. Szabo, A. Bax, L. E. Kay, P. C. Driscoll and A. M. Gronenborn, *J. Am. Chem. Soc.*, 1990, **112**, 4989–4991.
46 D. Idiyatullin, V. A. Daragan and K. H. Mayo, *J. Phys. Chem. B*, 2003, **107**, 2602–2609.
47 C. Charlier, S. N. Khan, T. Marquardsen, P. Pelupessy, V. Reiss, D. Sakellariou, G. Bodenhausen, F. Engelke and F. Ferrage, *J. Am. Chem. Soc.*, 2013, **135**, 18665–18672.
48 T. Zinkevich, V. Chevelkov, B. Reif, K. Saalwächter and A. Krushelnitsky, *J. Biomol. NMR*, 2013, **57**, 219–235.
49 J. R. Lewandowski, M. E. Halse, M. Blackledge and L. Emsley, *Science*, 2015, **348**, 578–581.
50 N. Giraud, M. Blackledge, M. Goldman, A. Bockmann, A. Lesage, F. Penin and L. Emsley, *J. Am. Chem. Soc.*, 2005, **127**, 18190–18201.
51 S. F. Lienin, T. Bremi, B. Brutscher, R. Bruschweiler and R. R. Ernst, *J. Am. Chem. Soc.*, 1998, **120**, 9870–9879.
52 Y. E. Shapiro and E. Meirovitch, *J. Phys. Chem. B*, 2012, **116**, 4056–4068.
53 J. Cavanagh, W. J. Fairbrother, A. G. I. Palmer, N. J. Skelton and M. Rance, *Protein NMR Spectroscopy*, Academic Press, 2nd edn, 2006.
54 J. Schaefer, R. A. Mckay and E. O. Stejskal, *J. Magn. Reson.*, 1979, **34**, 443–447.
55 S. Hediger, B. H. Meier and R. R. Ernst, *Chem. Phys. Lett.*, 1995, **240**, 449–456.

